Lab on a Chip

Miniaturisation for chemistry, physics, biology, materials science and bioengineering

www.rsc.org/loc

Volume 12 | Number 13 | 7 July 2012 | Pages 2279–2422

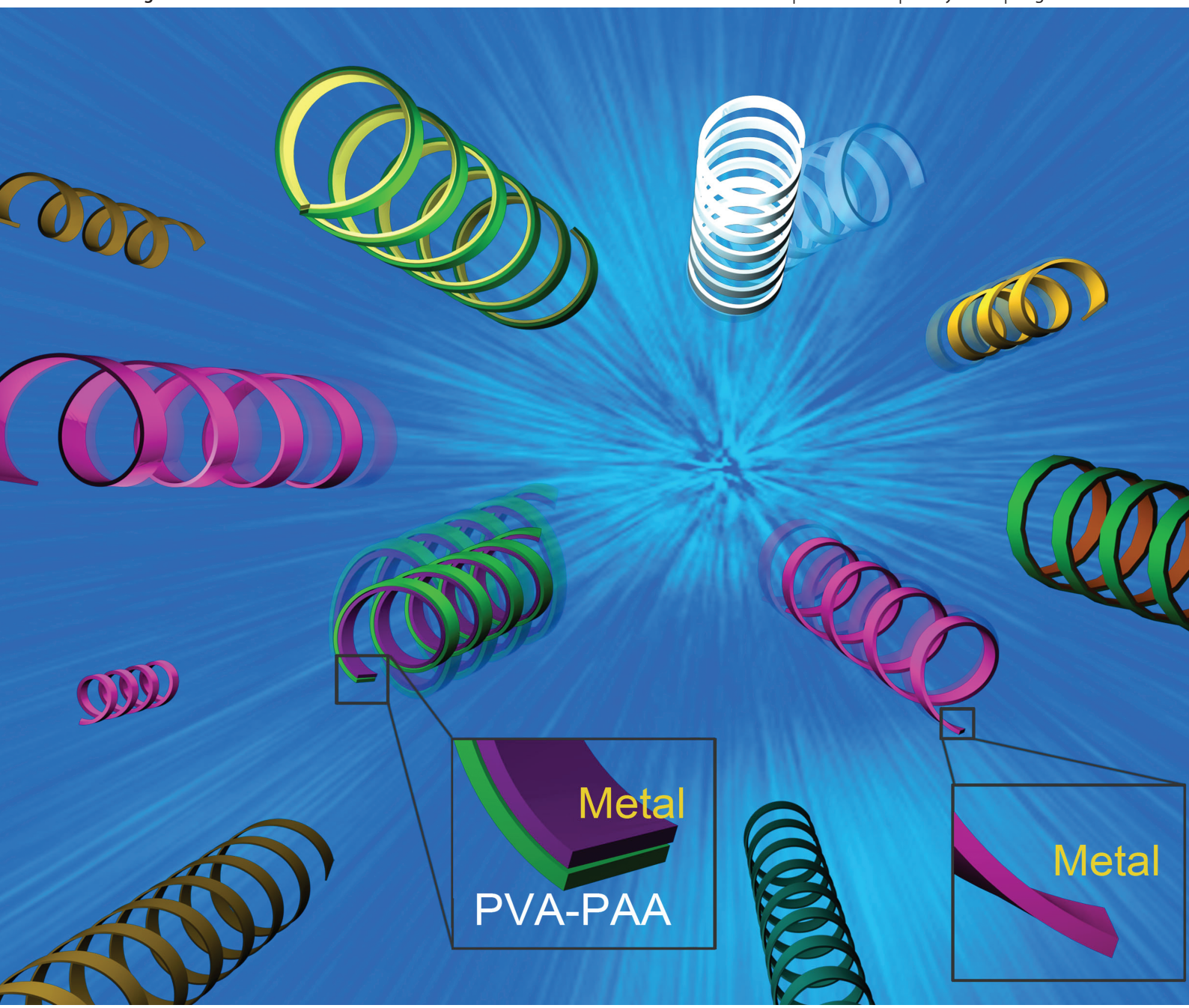

ISSN 1473-0197

RSC Publishing

PAPER

Weiming Li *et al.*

Superelastic metal microsprings as fluidic sensors and actuators

1473-0197(2012)12:13;1-#

Lab on a Chip

Dynamic Article Links

Cite this: *Lab Chip*, 2012, **12**, 2322–2328

www.rsc.org/loc

PAPER

Superelastic metal microsprings as fluidic sensors and actuators†

Weiming Li,‡[a] Gaoshan Huang,‡*[a] Jiao Wang,[a] Ying Yu,[a] Xiaojing Wu,*[a] Xugao Cui[b] and Yongfeng Mei*[ac]

Received 12th February 2012, Accepted 13th March 2012
DOI: 10.1039/c2lc40151g

Superelastic metal microsprings fabricated by deterministic rolling of nanomembranes have been anisotropic-strain-engineered *via* glancing angle deposition. The advantageous applications of metal microsprings in liquid flow rate sensors and chemical-stimulated actuators due to their reliable superelasticity are demonstrated. Theoretical calculation of microspring elongation as a function of flow rate agrees with our experimental observation and reveals that the sensitivity can be well tuned by the geometrical design of the microsprings. Such outstanding mechanical properties of rolled-up metal microsprings should find important applications in future fluidic micro-/nano-devices.

Introduction

Motivated by enormous progress in the miniaturization of mechanical, electronic, and opto-electronic devices, researchers in micro-/nano-sciences have put great effort into the fabrication and characterization of novel micro-/nano-structures.[1–3] Typical structures in the forms of dots,[4] wires,[5] tubes,[6,7] *etc.* have been intensively investigated in recent years and their potential applications in drug-delivery,[8] sensing,[9,10] optics,[11] micro swimmers,[12] and data storage[13] are being widely explored and developed. Among various micro-/nano-structures, springs or helices have drawn extensive research interest due to their unique three-dimensional geometry. Compared with simpler shapes, their structural complexities are more attractive because such geometry may have a remarkable effect upon their physical and chemical properties.[14–16] The excellent performance of devices consisting of micro-/nano-springs has already led to advantageous uses in micro-/nano-electromechanical systems,[17] targeted delivery,[18] sensing[19,20] and microelectronics.[21]

During the past few years, micro-/nano-springs have been fabricated from various materials, such as ZnO,[22] Si_3N_4,[23] C,[24] and SiO_2[25] *via* bottom-up methods *e.g.* solid–vapor process and chemical vapor deposition.[22,23,26] These structures are formed entirely through a self-assembly process and thus exhibit slightly less controllability. Recently, rolled-up nanotechnology, which exploits both bottom-up and top-down methods,[27] has been employed to fabricate three-dimensional structures by the rolling-up of pre-strained nanomembranes upon release from a sacrificial layer. In the beginning, this strain was introduced to bi-layered nanomembranes with a crystal lattice mismatch.[28,29] These materials systems such as InGaAs/GaAs bilayers and SiGe/Si bilayers were grown by chemical vapor deposition or by molecular beam epitaxy onto sacrificial layers.[6,19,30] For single-crystal semiconductor nanomembranes, Young's modulus is strongly anisotropic and nanomembranes with well-defined geometries will roll along the direction where Young's modulus is the smallest.[30] If the orientation of a nanomembrane strip deviates from this rolling direction, a helical structure is thus formed, which is in fact a special case of the rolled-up tube.[19] Researchers have demonstrated perfect helical structures using this method, and physical properties of obtained coils were carefully investigated.[6,17–19,21,30] It is noted, though, that the helicity angle cannot be smaller than 45° due to the constructive limitation of the Si crystal.[21] This restriction can only be overridden in very narrow strips due to the edge effect or with an additional isotropic Cr layer.[30] On the other hand, rolled-up nanotechnology can also be created by strain-engineering of nanomembranes on a polymer sacrificial layer, and a broad range of materials have been rolled.[31] However, metal nanomembranes fabricated by vapor deposition (*e.g.* evaporation and sputtering) are generally believed to be isotropic,[30,32,33] and thus it is difficult to obtain helical structures from pure metal nanomembranes since no preferential rolling direction can be precisely defined. In this work we report, for the first time, a convenient and robust methodology for fabricating pure metal microsprings *via* deterministic rolling of anisotropic strain-engineered nanomembranes deposited by evaporation on a polymer sacrificial layer. The mechanical behaviors of the obtained metal microsprings and their applications in fluid rate sensing and chemical-stimulated actuators have been studied in detail. We also reveal a superelasticity behavior (shape memory)[22] of our metal microsprings which is not observed in

[a]*Department of Materials Science, Fudan University, Shanghai, 200433, China. E-mail: gshuang@fudan.edu.cn; wuxj@fudan.edu.cn; yfm@fudan.edu.cn*
[b]*Department of Light Sources & Illuminating Engineering, School of Information Science & Engineering, Fudan University, Shanghai, 200433, China*
[c]*Key Disciplines Lab of Novel Micro-nano Device and systems Technology & Microsystem Research Center, Chongqing University, Chongqing, 400044, China*

† Electronic supplementary information (ESI) available: geometries of microsprings and their controllability, detailed calculation method, influence of geometry on *v*–*x* relationship, and videos. See DOI: 10.1039/c2lc40151g/

‡ These authors contributed equally to this work.

previous helical semiconductor structures. The outstanding mechanical and electrical properties of microsprings made of metal undoubtedly appear to be more suitable for potential applications in future micro-/nano-devices.

Experimental

Fabrication of metal microsprings

A poly(methyl methacrylate) (PMMA) sacrificial layer was deposited on the top of a Si substrate by spin-coating of 5% PMMA solution in toluene at a speed of 1800 rotations per minute, which was then patterned by photolithography or using adhesive tape as a shadow mask, and thus a step of sacrificial layer was formed on the substrate. Ti nanomembranes were subsequently deposited by e-beam evaporation under high vacuum ($<10^{-4}$ Pa) with glancing angles. The Ti nanomembranes were patterned into rectangles or strips by photolithography, using a shadow mask during the deposition, or even scratching with a sharp blade. Acetone was used for the etching process to release the Ti nanomembranes. The intrinsic stress in the anisotropic-strain-engineered Ti nanomembranes made them roll up and self-assemble into microtubular or microspring structures.

Fabrication of hybrid microsprings

A polyvinyl alcohol (PVA)–poly(acrylic acid) (PAA) nanomembrane with thickness of approximately 150 nm was spin-coated on the top of SiO_2, followed by a heating process for crosslinking reaction. Subsequently, a 50 nm thick Cr nanomembrane was deposited on the top of the polymer layer by e-beam evaporation under high vacuum ($<10^{-4}$ Pa) with glancing angles. Then, the hybrid bilayer nanomembrane was patterned by a sharp blade. A 5% HF solution was used to selectively remove the sacrificial SiO_2 layer releasing the hybrid nanomembrane. The microspring was then thoroughly rinsed by DI water. The PVA–PAA nanomembrane can swell in water which introduces additional isotropic strain/stress at the Cr/PVA–PAA interface.

Microscopy

The morphologies of rolled-up microtubes and microsprings were checked using optical microscopy (Olympus BX51) connected to a camera for high resolution color images.

Flow rate sensing

To investigate the mechanical behavior of microsprings in flow water, the Ti microsprings fixed on the top of Si substrates were placed into a glass conduit with a rectangular cross-sectional area of 2×4 mm^2. The morphologies of microsprings under flow rates ranging from 0 to 0.5 m s^{-1} were recorded by the real-time optical microscopy.

Characterization of chemical-stimulated actuator

The as-prepared hybrid microspring in water was fixed on the bottom of a petri dish. The solution in the petri dish was changed to check its influence on the geometry of the microspring, and the morphological evolution of the microspring was recorded by real-time optical microscopy.

Results and discussion

Fabrication of metal microsprings

Fig. 1a illustrates a general process for producing pure metal microsprings.[34] The basic scientific principle behind it is essentially the same as that of previous helical semiconductor structures, where the orientation of the strip must be misaligned with the direction of the anisotropic strain/stress.[19,21,30] In the present work, a sacrificial polymer layer is first deposited on the top of an Si substrate by spin-coating. It is noteworthy in panel i of Fig. 1a that only part of the substrate is covered by the sacrificial layer through patterning (*e.g.* by photolithography or using a shadow mask), which forms a step on the substrate. An anisotropic metal nanomembrane is then deposited onto the substrate and the sacrificial layer. In order to obtain microsprings after removal of the sacrificial layer, the metal nanomembrane needs to be patterned into strips beforehand, as demonstrated in panel ii of Fig. 1a. It is important to make sure that the orientation of the metal strips is intentionally misaligned to the anisotropic strain/stress direction (the x axis in Fig. 1a) with an angle of α. The misaligned metal strips are finally released from the sacrificial layer *via* an under-etching process.[35] As shown in panel iii of Fig. 1a, the organic solvent effectively removes the polymer sacrificial layer releasing the metal strips, and the stress in direction x simultaneously leads to microspring formation by causing anisotropic strain. One may note that the metal nanomembrane directly deposited on top of the substrate remains unaffected during etching, and thus the formed metal microsprings are fixed to the substrate at one end.

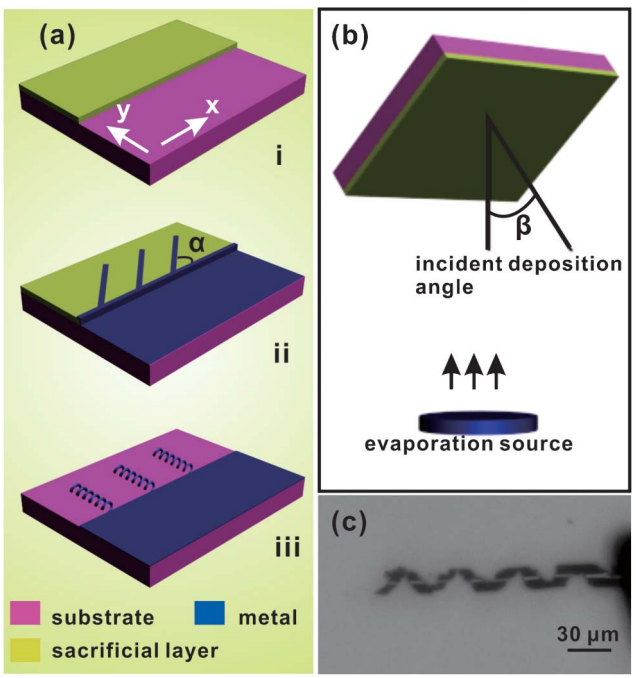

Fig. 1 (a) A general process used to fabricate metal microsprings. (b) Schematic diagram of glancing angle deposition. (c) Optical microscope image of a Ti microspring.

We should stress that the fixing of microsprings onto a substrate is quite useful in the accurate positioning and integration of microsprings on a single chip, and this is also of benefit to the applications discussed later.

Obviously, the most important part of the process is to introduce strain anisotropy in the metal nanomembrane deposited by evaporation, which was previously considered to be a serious stumbling block.[30] We successfully solve this problem by engaging glancing angle deposition (GLAD) which has been used to obtain films consisting of nanopillars/nanorods with dimensions measuring tens of nanometers due to an atomic shadowing effect under limited adatom mobility conditions.[36,37] Fig. 1b schematically shows the configuration corresponding to GLAD employed in our work. The sample is fixed on the sample holder and the normal direction of the sample surface is set to an angle β with respect to the direction of material flux during deposition (see Fig. 1b). We have found this approach can effectively introduce anisotropy into the nanomembrane, and the strips cut from the nanomembrane deterministically roll up into microspring structures.[34] An optical image of a typical Ti microspring fabricated using the above approach is shown in Fig. 1c, which validates the feasibility of our method.

To demonstrate anisotropic-strain-engineering of pure metal nanomembranes deposited by GLAD in a distinct way, we have carried out the verification experiment shown schematically in Fig. 2. After fabrication of the sacrificial polymer layer, Ti nanomembranes were deposited with an incident deposition angle $\beta = 60^\circ$. The thickness of the nanomembrane is set to be 40 nm with a uniform deposition rate of 4 Å s^{-1}. The strain gradient in the Ti nanomembranes is induced due to the difference in thermal expansion between the sacrificial layer and the Ti nanomembrane during GLAD, as we have demonstrated in previous work.[31] In order to test the rolling direction determined by anisotropic-strain-engineering of the Ti nanomembrane, the original nanomembrane is patterned into rectangular shapes with orientations perpendicular to each other (see Fig. 2a). The short sides of the rectangles of the first pattern (upper row in Fig. 2a) are parallel to the x-axis, which is perpendicular to the incident direction as depicted in Fig. 1b. In contrast, the short sides of the rectangles of the second pattern (lower row in Fig. 2a) are perpendicular to the x-axis. It is shown experimentally that upon release, nanomembranes in both cases rolled up along the x-axis, forming microtubes aligned to the same direction (Fig. 2b and 2c), despite the significant geometrical difference between the two patterns. It was previously reported that the geometry of the nanomembrane affects the rolling direction for a rectangular-shaped membrane with isotropic strain/stress, and that long side rolling always produces the lowest energy state.[38] However, in the current experiment the rolling behavior of the Ti nanomembranes deposited by GLAD is proven to be independent of geometry. The rolling direction is exclusively dominated by the incident direction during GLAD, *i.e.* the rolling direction is always vertical to the incident direction, which strongly suggests the anisotropy of strain in the produced Ti nanomembranes. It is worth noting that a directional rolling behaviour has also been observed before by introducing a slight surface modulation to the nanomembranes.[39] However, in our present experiment, post-treatment is not engaged after e-beam evaporation and morphological characterization did not show any surface modulation, indicating the anisotropic strain/stress was intrinsically introduced during nanomembrane deposition. The detailed mechanism corresponding to this unique anisotropic property in the Ti nanomembrane is so far not clearly specified, nevertheless, anisotropy in Young's modulus and strain/stress are believed to be intimately connected with the structural asymmetry produced by the shadow effect in GLAD.[36,37]

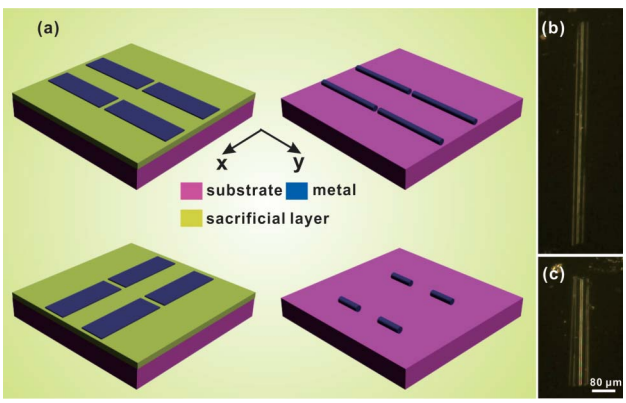

Fig. 2 (a) Schematic diagram illuminating the experiments used to demonstrate anisotropic-strain-engineering of the metal nanomembrane deposited by GLAD. Optical microscope images of Ti microtubes rolled up from the long side (b) and the short side (c) of the rectangles. See main text for more details.

Design of metal microsprings

Since the nanomembranes can be anisotropic-strain-engineered by the flux direction during GLAD, we can easily design microsprings with varied helicity angles as long as a misaligned angle α (see panel ii in Fig. 1a) between the orientation of the strip and the "soft" direction exists.[21,38] To better evaluate the geometrical structure of the obtained microspring, several parameters such as the radius R, the pitch p, and the helicity angle θ were chosen for characterization purposes. The definitions of these parameters are graphically illustrated in the inset of Fig. 3b, and their values are R_0, p_0, and θ_0, respectively, when the microspring is relaxed. The relationship of these parameters is determined by the geometry restriction:

$$2\pi R \tan\theta = p \quad (1)$$

Thus the helicity angles θ_0 can be calculated using eqn (1) and compared among different microsprings. We prepared a number of microspring samples with different geometries in our experiment by tuning the misaligned angles from 20° to 75°. Fig. 3a shows the optical microscope images of three typical Ti microsprings with different calculated helicity angles of 20°, 50°, and 75°. The perfect geometry of the microsprings is clearly visible. Fig. 3b illustrates the relationship between θ_0 and α derived from our microscopy observation (see Table S1, ESI†), and we found that θ_0 is always equal to α with small experimental uncertainty. This further proves the deterministic rolling along the direction of the x-axis (see the inset of Fig. 3b for more details). It is worth noting that when the misaligned angle is 0° or 90°, the strips can roll into microtubes (as exhibited in Fig. 2b

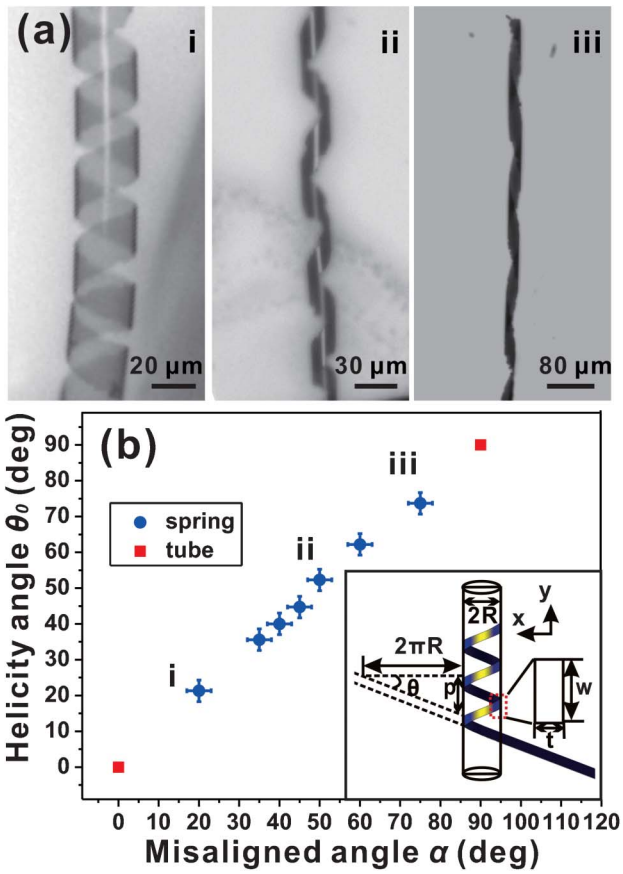

Fig. 3 (a) Optical microscope images of Ti microsprings with helicity angles of (i) 20°, (ii) 50°, and (iii) 75°. (b) Helicity angle of the microspring (θ_0) as the function of the misaligned angle (α) between the orientation of the strip and the x-axis. The results corresponding to the structures shown in (a) are labelled. The inset illustrates the definition of the parameters of the microspring structure.

and 2c, or into microrings if the strips are narrow enough) rather than microsprings. In previous helical semiconductor structures, the helicity angle is inherently larger than 45° due to equivalent <100> directions of silicon crystal, and smaller angles could only be achieved by using a narrow strip or adding an additional Cr layer.[21,30] Such limitations do not exist in the present case because there is only one preferred rolling direction, *i.e.* along the x-axis, which makes it possible to fabricate microsprings of single materials with θ_0 in a large range, independent of the strip width. In addition, our approach of microspring fabrication also demonstrates good controllability in geometry tuning compared to previous work.[20] For instance, the diameter and the chirality of the microsprings can be controlled by altering the thickness and the orientation of the original metal strips (see Fig. S1 and Fig. S2 for more details, ESI†).

Application in liquid flow rate sensing

The mechanical properties of Ti microsprings in flowing water were studied using a device illustrated in the inset of Fig. 4, where the microspring fixed on the substrate is placed in the center of a glass conduit filled with flowing water. The real-time geometrical change of the microspring can therefore be observed and recorded by optical microscopy. The experimental relationships between

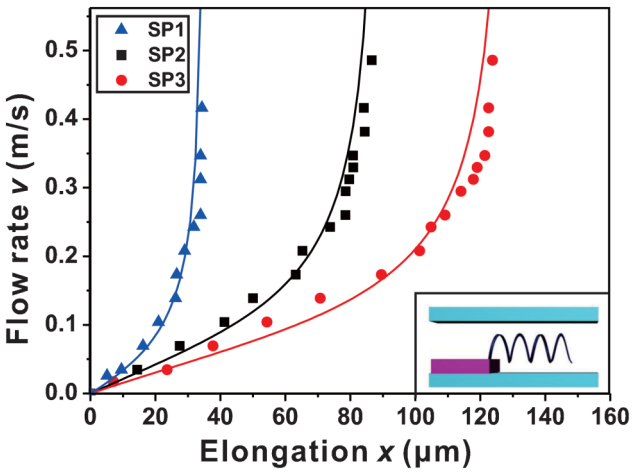

Fig. 4 Relationship between the flow rate (v) and the elongation of the Ti microsprings (x). The triangles, squares, and circles are experimental results from three different Ti microsprings (SP1: n = 2.0; SP2: n = 3.5; SP3: n = 4.8) and the solid lines in different colors are from theoretical calculations fitted to corresponding experimental results. The inset shows the schematic illustration of the device used to investigate the mechanical properties of Ti microsprings in flowing water.

the elongation (x) and the flow rate (v) for three different Ti microsprings with R_0 of ~10 μm are shown in Fig. 4 using triangles, squares, and circles, respectively. One can see that the elongation increases with the flow rate when the elongation is relatively small, but gradually becomes saturated at large elongations, where the microsprings have been stretched to shapes close to their original morphologies *i.e.* strips. This will be discussed later to show the superelasticity of the Ti microsprings.

In the following part, we will try to understand the mechanical properties of the microspring by theoretical calculations based on its unique geometry. In flowing water, the microspring is subjected to the drag force (F_D), which is balanced by the elastic force (F_E). The drag force applied onto the microspring is rather complicated and for simplification purposes, we assume that the spring is a part of circular cylinder. Thus F_D is considered to be parallel to the surface and proportional to the surface area. In the case of a cylindrical structure, the drag force $F_{D,cylinder}$ is in the form of

$$F_{D,cylinder} = \frac{2\pi\mu L v}{\ln\left(\frac{2L}{R}\right) - 0.72} \quad (2)$$

where μ is the viscosity of the fluid, ~0.001 Pa s for water in the present case, and L and R are the length and radius of the corresponding cylinder, respectively.[40] Correspondingly, F_D on a microspring can be expressed as:

$$F_D = F_{D,cylinder}\frac{S_{spring}}{S_{cylinder}} = \left[\frac{2\pi\mu L v}{\ln\left(\frac{2L}{R}\right) - 0.72}\right]\frac{2lw}{2\pi RL} = \frac{2\mu lw}{\left[\ln\left(\frac{2L}{R}\right) - 0.72\right]R}v \quad (3)$$

where S_{spring} is the surface area of the microspring (two sides), $S_{cylinder}$ is the side area of the cylinder (one side), and l and w the length and the width of the original metal strip, respectively.

Assuming that the spring is rolled from a metal strip with a rectangular cross-section and considering that the geometry of the spring is symmetric, we thus write the spring constant k_0 for one cycle of the microspring as follows:[22]

$$\frac{1}{k_0} = \frac{4\pi^2}{Gtwl_0} \left\{ \frac{p^2}{8\pi^2(1+\upsilon_{\text{Poisson}})t^2}\left(t^2+12R^2\right) + R^2\left[\frac{7+6\upsilon_{\text{Poisson}}}{6(1+\upsilon_{\text{Poisson}})} + \frac{12R^2}{t^2+w^2}\right]\right\} \quad (4)$$

where G is the shear modulus, t and w represent the dimensions of the cross-sectional area of the original strip as illustrated in the inset of Fig. 3b (*i.e.* the thickness and the width of the strip, respectively), l_0 is the total length of a unit cycle of the microspring (the number of cycles $n = l/l_0$), and $\upsilon_{\text{Poisson}}$ the Poisson's ratio. As the thickness of the metal strip is 40 nm, which is far smaller than R, p and w, the spring constant k_0 of a single cycle of the microspring can be simplified as:

$$\frac{1}{k_0} = \frac{4\pi^2}{Gtwl_0}\frac{p^2}{8\pi^2(1+\upsilon_{Poisson})t^2}12R^2 = \frac{6p^2R^2}{G(1+\upsilon_{\text{Poisson}})t^3wl_0} \quad (5)$$

and the spring constant k for a spring with n cycles can be expressed as:

$$\frac{1}{k} = \frac{6np^2R^2}{G(1+\upsilon_{\text{Poisson}})t^3wl_0} \quad (6)$$

Similar to previous work,[41] the spring constant k is defined as the elastic force divided by the x:

$$F_{\text{E}} = kx \quad (7)$$

Obviously, if the microspring is stationary in the flowing water, F_{D} and F_{E} are equal, thus combining eqn (3), (6), and (7), we obtain:

$$\frac{x}{v} = \frac{12\mu n^2p^2R}{G(1+\upsilon_{\text{Poisson}})\left[\ln\left(\frac{2L}{R}\right)-0.72\right]t^3} \quad (8)$$

Considering the geometrical relationship of the microspring (see ESI† for more details), we finally get the relationship between v and x by assuming n is a constant during the deformation process:[22]

$$v = \frac{\pi G(1+\upsilon_{\text{Poisson}})t^3}{6\mu} \times \frac{\ln\left[\frac{4\pi(np_0+x)}{\sqrt{4\pi^2R_0^2+p_0^2-\frac{(np_0+x)^2}{n^2}}}\right]-0.72}{(np_0+x)^2\sqrt{4\pi^2R_0^2+p_0^2-\frac{(np_0+x)^2}{n^2}}}x \quad (9)$$

The solid curves in Fig. 4 showing the increase of v as a function of x are derived from eqn (9), where the values of G and $\upsilon_{\text{Poisson}}$ of the Ti nanomembrane are assumed to be the same as those of bulk Ti, *i.e.* 44 GPa and 0.33,[42] respectively. Details concerning the theoretical calculation can be found in the ESI.† The three theoretical curves show good agreement with the experimental data (See Fig. S3, ESI†). However, a small deviation was observed for large v and corresponding large x. The inconsistency between the experimental and theoretical results is believed to be due to the gradual decrease of n, especially for extremely elongated microsprings since n is taken to be a constant in our calculation.

The elongation of the microspring in the flowing water suggests a potential application in flow rate sensing since the elongation can be easily detected by optical or electrical means. Here, we can calculate the sensitivity (S) of this kind of flow rate sensors by

$$S = \frac{dx}{dv} \quad (10)$$

According to eqn (9) and (10) and the curves in Fig. 4, the highest sensitivity our microspring-based flow rate sensor achieved is $\sim$500 μm/(m s^{-1}). Correspondingly, the detection limit of this sensor is determined to be 0.002 m s^{-1}, from the 1 μm resolution of the optical microscopy. The geometry of the microspring has an important influence on its mechanical properties and sensitivity. We calculated the elongation, x, of microsprings with different pitch, p_0, and number of cycles, n, in flowing water (Fig. S4, ESI†). The results demonstrated a significant influence on x from n whereas a change in p_0 has little effect. With the same flow rate, v, the microspring with a big n will be largely elongated, indicating a better sensitivity. Therefore, the microspring with more cycles is more suitable for smaller flow rates since the consequent larger elongation can be more easily detected.

Superelasticity of rolled-up metal microsprings

A superelasticity behavior (shape memory) of Ti microsprings was found in our experiment (see the video in the ESI†). Fig. 5a records the sequential large extension and superelastic recovery process of the Ti microspring in different flow rates. The Ti microspring was first stretched from its original relaxed state (panel i in Fig. 5a, v = 0 m s^{-1}) to its maximum extension (panel ii in Fig. 5a, v = 0.3 m s^{-1}), and then completely recovered after the flow rate was decreased to 0 (panel iii in Fig. 5a). One can see that the recovered microspring shows identical dimensionality including pitch and radius, suggesting a superelasticity behavior.[22,23] A reliability test of the superelasticity behavior of Ti microsprings was carried out in flowing water with the flow rate altered periodically. Fig. 5b shows the length of the microspring as a function of the flow rate in 12 cycles. The microspring is still completely recoverable to its original geometry without any deterioration, indicating a good reliability of the superelasticity behavior. An obvious advantage demonstrated is the excellent mechanical properties of the present metal microsprings, which are mainly ascribed to the good ductility of metal and thus cannot be easily obtained from semiconductor microsprings.

Application in chemical-stimulated actuators

To further demonstrate that the superelastic metal microspring can be used to detect the concentration alteration in the liquid (*i.e.* as a chemical-stimulated actuator), we prepared hybrid

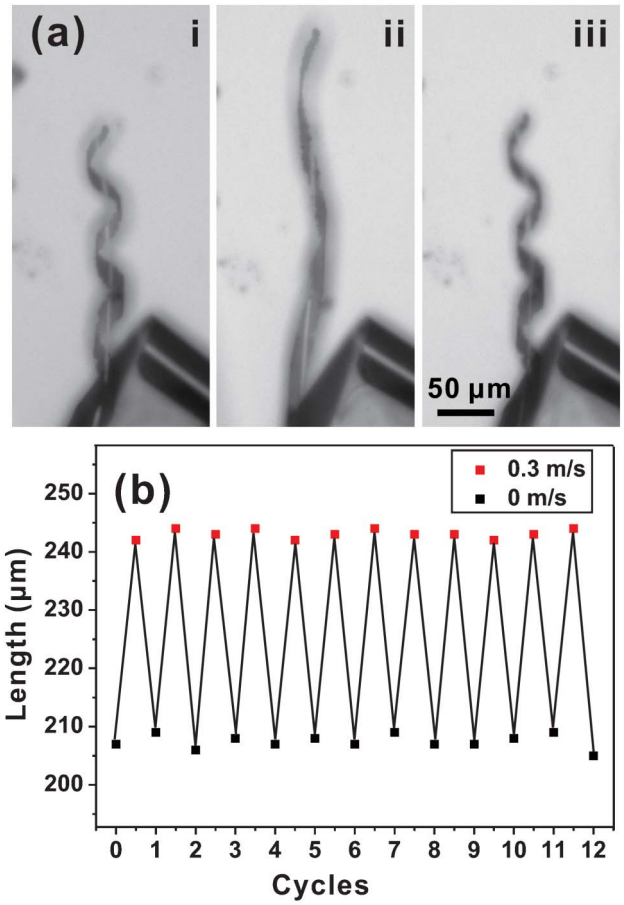

Fig. 5 (a) Optical microscope images of a Ti microspring during one cycle of extremely large extension and superelastic recovery with different flow rates: (i) 0, (ii) 0.3, and (iii) 0 m s^{-1}. (b) Experiment illustrating the reliable superelasticity of the microspring in 12 cycles.

microspring from Cr/hydrogel. The hydrogel used here is PVA–PAA, which has a strong swelling ability and thus can be used as a sensing material to detect certain molecules due to its sensitive volume change.[43,44] However, the quantitative analysis of the volume change directly is challenging. The combination of this material with the Cr microspring thus provides a convenient way to reflect the volume change distinctly because the volume change introduces additional isotropic strain/stress at the interface and consequently contributes to morphological evolution of the microspring. That is to say, the hybrid microspring was used as a simple transducer to transform the volume change into a geometrical change of the microspring which was then probed by optical microscopy. Fig. 6a and the video in the ESI† show the corresponding experimental results. One can see the hybrid microspring starts to unroll when being transferred from water to ethanol at 0 s and the number of rotations gradually decreases from ~2 to ~1 along with the radius increasing from 22 to 45 μm (20 s in Fig. 6a). The morphological evolution is due to the deswelling behavior of the PVA–PAA which removes the influence of the additional strain/stress introduced when the microspring was immersed in the water. It is worthwhile to note that the bilayer stripe keeps its helical shape instead of a stripe with prolonged immersion time in ethanol, which is considered to be due to the anisotropic-strain-engineered Cr nanomembrane, as we have discussed previously. After water was added to the ethanol at 36 s (volume ratio of water to ethanol is 1 : 10), the microspring rolled tighter with decreasing radius, and the original geometry is ultimately restored within ~15 s (video in the ESI† and the plot in Fig. 6b), suggesting such a hybrid microspring can be used as a chemical-stimulated actuator.[44] The present results demonstrate excellent flexibility of our metal-based microspring, and the approach can be easily combined with other techniques to obtain micro-/nano-structures for a broad range of applications.

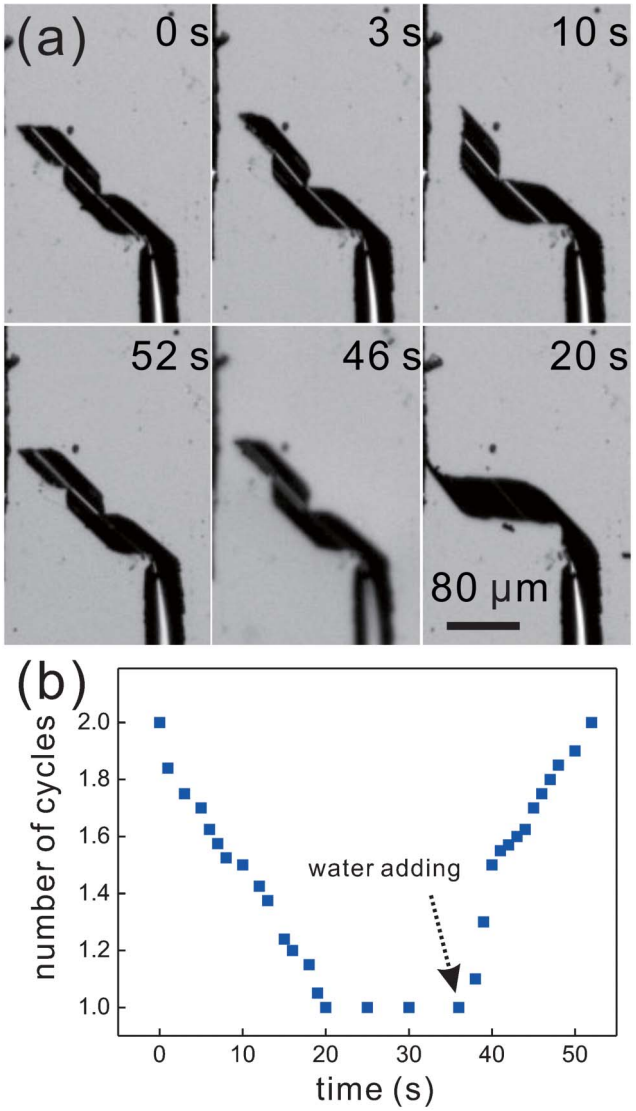

Fig. 6 (a) Optical microscope images of a Cr/PVA-PAA hybrid microspring used as a chemical-stimulated actuator. Upper row: unrolling of the microspring in ethanol. Lower row: rolling of the microspring in water : ethanol mixture (1 : 10 in volume). (b) The number of rotations of the microspring as a function of time. The value is obtained from the real-time video, ESI.†

Conclusions

In conclusion, we have demonstrated a convenient and robust method to fabricate pure metal microsprings with helicity angles varied from 20° to 75° by deterministic rolling of anisotropic-

strain-engineered nanomembranes prepared by GLAD. The microsprings are found to stretch in flowing water due to the drag force, and the elongation as a function of flow rate is observed experimentally and can be well predicted by theoretical calculations, indicating potential applications of the metal microsprings in flow rate sensing. The superelasticity behavior of Ti microsprings and the corresponding reliability was demonstrated after more than 10 cycles of extremely large extension and superelastic recovery (shape memory). We further disclosed the water–ethanol chemical-stimulated actuators application of the Cr/PVA–PAA microspring. The excellent mechanical and electric properties of metal itself, as well as the superelastic property, suggest a great number of potential applications for metal microsprings in micro-/nano-electromechanical systems.[45]

Acknowledgements

This work is supported by the Natural Science Foundation of China (Nos. 61008029, 51102049, 51103027, and 11104040), Program for New Century Excellent Talents in University (No. NCET-10-0345), and "Shu Guang" project by Shanghai Municipal Education Commission and Shanghai Education Development Foundation. YFM also thanks the support from the Visiting Scholar Foundation of Key Laboratory of Optoelectronic Technology and Systems in Chongqing University.

References

1 J. A. Rogers, M. G. Lagally and R. G. Nuzzo, *Nature*, 2011, **477**, 45.
2 Y. F. Mei, A. A. Solovev, S. Sanchez and O. G. Schmidt, *Chem. Soc. Rev.*, 2011, **40**, 2109.
3 A. Cho, *Science*, 2006, **313**, 164.
4 H. J. Jeon, Y. K. Baek, S. B. Yang, S. K. Lee, J. M. Jung and H. T. Jung, *J. Mater. Chem.*, 2011, **21**, 14285.
5 Y. F. Hu, Y. Zhang, C. Xu, G. Zhu and Z. L. Wang, *Nano Lett.*, 2010, **10**, 5025.
6 M. H. Huang, C. Boone, M. Roberts, D. E. Savage, M. G. Lagally, N. Shaji, H. Qin, R. Blick, J. A. Nairn and F. Liu, *Adv. Mater.*, 2005, **17**, 2860.
7 I. S. Chun, V. B. Verma, V. C. Elarde, S. W. Kim, J. M. Zuo, J. J. Coleman and X. Li, *J. Cryst. Growth*, 2008, **310**, 2353.
8 A. A. Solovev, S. Sanchez, M. Pumera, Y. F. Mei and O. G. Schmidt, *Adv. Funct. Mater.*, 2010, **20**, 2430.
9 Q. Yang, X. Guo, W. Wang, Y. Zhang, S. Xu, S. H. Lien and Z. L. Wang, *ACS Nano*, 2010, **4**, 6285–6291.
10 R. Attia, D. C. Pregibon, P. S. Doyle, J.-L. Viovy and D. Bartolo, *Lab Chip*, 2009, **9**, 1213.
11 S. Mendach, R. Songmuang, S. Kiravittaya, A. Rastelli, M. Benyoucef and O. G. Schmidt, *Appl. Phys. Lett.*, 2006, **88**, 111120.
12 A. Ghosh and P. Fischer, *Nano Lett.*, 2009, **9**, 2243.
13 A. J. Hong, C. C. Liu, Y. Wang, J. Kim, F. Xiu, S. Ji, J. Zou, P. F. Nealey and K. L. Wang, *Nano Lett.*, 2010, **10**, 224.
14 L. Liu, S. H. Yoo, S. A. Lee and S. Park, *Nano Lett.*, 2011, **11**, 3979.
15 J. K. Gansel, M. Thiel, M. S. Rill, M. Decker, K. Bade, V. Saile, G. von Freymann, S. Linden and M. Wegener, *Science*, 2009, **325**, 1513.
16 E. J. Smith, D. Makarov, S. Sanchez, V. M. Fomin and O. G. Schmidt, *Phys. Rev. Lett.*, 2011, **107**, 097204.
17 D. J. Bell, Y. Sun, L. Zhang, L. X. Dong, B. J. Nelson and D. Grützmacher, *Sens. Actuators, A*, 2006, **130**, 54.
18 L. Zhang, K. E. Peyer and B. J. Nelson, *Lab Chip*, 2010, **10**, 2203.
19 D. J. Bell, L. Dong, B. J. Nelson, M. Golling, L. Zhang and D. Grützmacher, *Nano Lett.*, 2006, **6**, 725.
20 E. J. Smith, D. Makarov and O. G. Schmidt, *Soft Matter*, 2011, **7**, 11309.
21 L. Zhang, E. Deckhardt, A. Weber, C. Schönenberger and D. Grützmacher, *Nanotechnology*, 2005, **16**, 655.
22 P. X. Gao, W. Mai and Z. L. Wang, *Nano Lett.*, 2006, **6**, 2536.
23 C. Cao, H. Du, Y. Xu, H. Zhu, T. Zhang and R. Yang, *Adv. Mater.*, 2008, **20**, 1738.
24 K. W. Park, Y. E. Sung, S. Han, Y. Yun and T. Hyeon, *J. Phys. Chem. B*, 2004, **108**, 939.
25 H. F. Zhang, C. M. Wang, E. C. Buck and L. S. Wang, *Nano Lett.*, 2003, **3**, 577.
26 X. Y. Kong, Y. Ding, R. Yang and Z. L. Wang, *Science*, 2004, **303**, 1348.
27 I. S. Chun, K. Bassett, A. Challa and X. Li, *Appl. Phys. Lett.*, 2010, **96**, 251106.
28 V. Y. Prinz, V. A. Seleznev, A. K. Gutakovsky, A. V. Chehovskiy, V. V. Preobrazhenskii, M. A. Putyato and T. A. Gavrilova, *Phys. E.*, 2000, **6**, 828.
29 O. G. Schmidt and K. Eberl, *Nature*, 2001, **410**, 168.
30 L. Zhang, E. Ruh, D. Grützmacher, L. X. Dong, D. J. Bell, B. J. Nelson and C. Schönenberger, *Nano Lett.*, 2006, **6**, 1311.
31 Y. F. Mei, G. S. Huang, A. A. Solovev, E. Bermúdez-Ureña, I. Mönch, F. Ding, T. Reindl, R. K. Y. Fu, P. K. Chu and O. G. Schmidt, *Adv. Mater.*, 2008, **20**, 4085.
32 L. Zhang, R. Tu and H. Dai, *Nano Lett.*, 2006, **6**, 2785.
33 S. Heiroth, R. Ghisleni, T. Lippert, J. Michler and A. Wokaun, *Acta Mater.*, 2011, **59**, 2330.
34 W. M. Li, G. S. Huang, X. J. Wu and Y. F. Mei, *CN patent application*, 2011, 201110262186.4.
35 G. S. Huang, Y. F. Mei, D. J. Thurmer, E. Coric and O. G. Schmidt, *Lab Chip*, 2009, **9**, 263.
36 K. Robbie, M. J. Brett and A. Lakhtakia, *Nature*, 1996, **384**, 616.
37 S. V. Kesapragada, P. Victor, O. Nalamasu and D. Gall, *Nano Lett.*, 2006, **6**, 854.
38 I. S. Chun, A. Challa, B. Derickson, K. J. Hsia and X. Li, *Nano Lett.*, 2010, **10**, 3927.
39 P. Cendula, S. Kiravittaya, I. Mönch, J. Schumann and O. G. Schmidt, *Nano Lett.*, 2011, **11**, 236.
40 J. Happle and H. Brenner, *Low Reynolds Number Hydrodynamics*, Prentice Hall: Englewood Cliffs, NJ, USA, 1965.
41 X. Chen, S. Zhang, D. A. Dikin, W. Ding, R. S. Ruoff, L. Pan and Y. Nakayama, *Nano Lett.*, 2003, **3**, 1299.
42 C. Leyens and M. Peters, *Titanium and titanium alloys: fundamentals and applications*, Wiley-VCH, Weinheim, Germany, 2003.
43 J. Sorber, G. Steiner, V. Schulz, M. Guenther, G. Gerlach, R. Salzer and K. F. Arndt, *Anal. Chem.*, 2008, **80**, 2957.
44 G. Gerlach, M. Guenther, J. Sorber, G. Suchaneck, K. F. Arndt and A. Richter, *Sens. Actuators, B*, 2005, **111**, 555.
45 Feng Liu, M. G. Lagally and J. Zang, *MRS Bull.*, 2009, **34**, 190.

